J. Phys. B: At. Mol. Opt. Phys. 26 (1993) 3387–3401. Printed in the UK

Differential cross sections for single and double ionization of helium by protons and antiprotons

L Meng†, R E Olson†, R Dörner‡, J Ullrich§ and H Schmidt-Böcking‡

† Laboratory for Atomic and Molecular Research and Department of Physics, University of Missouri-Rolla, Rolla, MO 65401, USA

‡ Institut für Kernphysik, Universität Frankfurt, D-6000 Frankfurt am Main, Federal Republic of Germany

§ GSI, D-6100 Darmstadt, Federal Republic of Germany

Received 29 September 1992, in final form 30 April 1993

Abstract. Theoretical and experimental cross sections are presented for single and double ionization of He differential in the projectile scattering angle and the transverse energy of the outgoing recoil ion. A dynamical four-body classical trajectory Monte Carlo method that includes radial electron correlation is utilized to calculate total and differential cross sections for 300 and 500 keV protons and antiprotons in impact collisions with He. The azimuthal emission characteristics of electrons, recoil ion and projectile relative to each other are analysed to provide detailed information on the dynamical differences between single and double ionization and between proton and antiproton impact.

1. Introduction

In recent years, experiments and theoretical calculations have provided information on the effect of electron correlation in ionization processes. Several interesting results have been realized (see, for example, the review articles by Cocke and Olson 1991, Schultz *et al* 1991). Of these, Andersen *et al* (1986) showed that the cross section for double ionization of He by fast ($v \approx 10$ au) protons and antiprotons depended upon the sign of the charge. This was partially explained by classical trajectory Monte Carlo (CTMC) calculations (Olson 1987) as an effect of the transient destabilization of the helium atom due to the difference in screening by the proton or antiproton. These calculations also indicated that a theoretical model, which includes all the four-body interactions, must be used to explain the enhanced double ionization cross section for antiprotons relative to that of protons. With the forced-impulse method that allows direct electron–electron interaction during short time segments, quantitative agreement with the experimental findings were first obtained for the ratio of double to single ionization cross sections (Ford and Reading 1988, Reading and Ford 1987).

Further, cross sections differential in the projectile scattering angle have been investigated by Giese and Horsdal (1988) and a peak near 1.0 mrad was found in the angular dependence of the ratio of double ionization to single-plus-double ionization cross section (the so called charge-state fraction, $F = \sigma^{++}/(\sigma^{+}+\sigma^{++})$). The *n*CTMC calculations by Olson *et al* (1989) and Born approximation calculations by Salin (1989, 1991) both indicate that the experimental observations are compatible with the independent electron model (McGuire and Weaver 1977), and that the peak in the charge-state fraction is due to incoherent scattering of the proton off both electrons of He. Although the latter calculations provide a correct angular dependence of the charge-state fraction on the projectile polar

0953-4075/93/193387+15$07.50

scattering angle, the magnitude given by these calculations is two to three times higher than that of experiment.

Based on the forced-impulse method, Reading *et al* (1989) suggested that the peak structure is caused by two incoherent collisions of the proton with the target electron that produce slow and fast electrons, and found a peak near 0.5 mrad for a proton energy of 1 MeV. In the more recent publication of Fang and Reading (1991), different peak positions of the charge state fraction with angle are obtained depending on the relative strength of the two soft electron, shake off, and two hard hit mechanisms, and it is found that such a combination of the individual mechanisms does not display a peak in the right place and at the correct height. However, a peak in the ratio is obtained at an angle of ~ 1.0 mrad in the two hard hit mechanism for the MeV impact range.

A newly developed recoil-ion coincidence technique has led Dörner *et al* (1989) to study the complete three-body transverse momentum exchange between the projectile, target nucleus, and electron in p + He single-ionization collisions at 500 keV. These authors showed that the recoil-ion energy distribution as a function of the projectile scattering angle strongly deviates from that given by a two-body interaction and demonstrated that the coupling of electronic and nuclear degrees of motion must be included for an accurate description of the collision dynamics. Moreover, it is shown that the CTMC method provides a convenient framework to understand the dynamics of ionization involving all four bodies in the collisions of protons and antiprotons with He.

In search of a method that can more accurately accommodate the experimental observations and theoretical predictions, we employ in this work the dynamical classical trajectory Monte Carlo method (dCTMC) as proposed by Montemayor and Schiwietz (1989) and summarized below in section 2. The dCTMC method includes radial correlation between electrons.

We note that the independent-event model used in the works by Crothers and McCarroll (1987) and Deb and Crothers (1990, 1991) provides good agreement with experiment for the total cross section of double ionization of helium by protons. However, this method has not been applied to differential measurements which give an increased understanding of the possible collision mechanisms.

In section 3, we have used the dCTMC method to analyse total and differential cross sections, charge-state fractions and recoil-ion energy distributions as a function of the laboratory projectile polar scattering angle θ_p for single and double ionization processes. Both 300 and 500 keV proton and antiproton impact collisions are considered. Experimental results of Dörner and collaborators are compared to our calculations along with those of other authors. Furthermore, we give the ionization cross sections differential in the azimuthal angle between the outgoing particles for 500 keV protons. This analysis helps provide a clear picture of the ionization mechanisms. Atomic units are used unless otherwise indicated.

2. Theory

The classical trajectory Monte Carlo (CTMC) method, as used in the present work, was developed by Abrines and Percival (1966), Percival and Richards (1975) and Olson and Salop (1977). Reinhold and Falcón (1986) provided a procedure for generating initial conditions for collisions with the helium atom; this procedure is employed in our work, in a four-body, three-dimensional collision context. Further, the screening parameters of the target electrons are varied during the collision according to their binding energy in an attempt to incorporate radial correlation directly into the time evolution of each collision (Montemayor and Schiwietz 1989).

The interaction between the four particles involved in the collision, namely, the projectile, the target nucleus, and the two target electrons are treated exactly as the sum of two-body Coulomb interactions. The Hamiltonian of the collision system has the form

$$H = \frac{p_t^2}{2m_t} + \frac{p_p^2}{2m_p} + \frac{p_1^2}{2m_e} + \frac{p_2^2}{2m_e} + \frac{Z_p Z_t}{|r_p - r_t|} - \frac{Z_p}{|r_1 - r_p|} - \frac{Z_p}{|r_2 - r_p|} - \frac{Z_t}{|r_1 - r_t|} - \frac{Z_t}{|r_2 - r_t|} + V_{12}(r_1, r_2) \tag{1}$$

where p_p, p_t, p_i, r_p, r_t, and r_i, $i = 1, 2$, are the momenta and coordinates of the projectile, the target nucleus and the target electrons, respectively. The charges of the projectile and the target nucleus are Z_p and Z_t, respectively. The Coulomb potential between the two electrons, V_{12}, can be approximated by a sum of potentials of each individual electron due to the screening of the target nucleus by the other electron,

$$V_{12} = V_1 + V_2 \tag{2}$$

with

$$V_1 = V(r_1) = \frac{1 - (1 + \lambda_2|r_1 - r_t|)\exp(-2\lambda_2|r_1 - r_t|)}{|r_1 - r_t|} \tag{3a}$$

$$V_2 = V(r_2) = \frac{1 - (1 + \lambda_1|r_2 - r_t|)\exp(-2\lambda_1|r_2 - r_t|)}{|r_2 - r_t|}. \tag{3b}$$

In equations (3*a*) and (3*b*), λ_1 and λ_2 represent the screening of the target nucleus by electrons 1 and 2, respectively.

Substituting equation (3) into equation (1) gives a model potential Hamiltonian equation that we use for the collision systems under consideration. Initially, λ_1 and λ_2 are set equal and take a value of $\lambda_{1s} = 1.6875$, as given by variational calculations of the ground-state binding energy of the helium atom. During the course of the collisions, the values of λ_1 and λ_2 vary linearly with the binding energy, E_j, $j = 1, 2$, of electron 1 and 2 as follows (Montemayor and Schiwietz 1989)

$$\lambda_j = \begin{cases} 0 & \text{for } E_j > 0 \\ \dfrac{\lambda_{1s}}{E_{1s}} E_j & \text{for } E_{1s} < E_j \leqslant 0 \\ \lambda_{1s} & \text{for } E_j \leqslant E_{1s} \end{cases} \qquad j = 1, 2. \tag{4}$$

By varying the screening parameters λ_1 and λ_2, when one electron is ionized, the other electron will be bound more tightly to the nucleus than prior to the collision. The initial binding energy, E_{1s}, of each electron on He, takes the value of 0.896 au. The method is termed dCTMC for dynamical CTMC.

One tool we use to elucidate the dynamics of single and double ionization is the calculation of polar and azimuthal angular differential cross sections for the various outgoing reaction products. The differential cross section for the projectile scattering angle θ_p is calculated as

$$\frac{d\sigma}{d\theta_p} = \pi b_{max}^2 \frac{N(\theta_p)}{N_T \Delta\theta_p} \tag{5}$$

where $N(\theta_p)$ is the number of reaction events for a specific final state in a scattering angle of $\theta_p \pm \frac{1}{2}\Delta\theta_p$, and b_{max} is the impact parameter beyond which the probability for this reaction is negligible, while N_T is the total number of trajectories integrated.

If we define the impact direction as that of the z-axis and the azimuthal angle of a vector, ϕ, as the angle between the projection onto the x–y plane of the vector and the x-axis, then a doubly differential cross section can be written as

$$\frac{d^2\sigma_p}{d\phi\, d\theta_p} = \pi b_{max}^2 \frac{N(\phi, \theta_p)}{N_T \Delta\phi \Delta\theta_p} \tag{6}$$

where $N(\phi, \theta_p)$ is the number of events associated with an azimuthal scattering angle $\phi \pm \frac{1}{2}\Delta\phi$ and a polar projectile scattering angle $\theta_p \pm \frac{1}{2}\Delta\theta_p$. In this work, ϕ represents the post-collisional azimuthal angle between outgoing particles in the plane perpendicular to the initial velocity vector of the projectile.

3. Experiment

The experiment was performed at the 2.5 MeV Van de Graaff accelerator of the Institut für Kernphysik, Universität Frankfurt. The incoming proton beam was collimated to a divergence of less than 0.1 mrad, passed through the gas cell (10^{-1} hPa) of the recoil-ion momentum spectrometer (RIMS) and was detected 2.7 m downstream by a two-dimensional position sensitive channel plate detector. Recoil ions, produced in the cylindrical cell of 10 mm in diameter and 40 mm long, drift from the beam axis to the wall of the cylinder. Upon exiting the cylinder through a slit (1 mm × 20 mm), they are post-accelerated, charge state analysed in a magnetic field and focused onto a two-dimensional position sensitive channel plate detector. The coincidence with the signal of the scattered projectiles yields the recoil-ion drift time in the cylinder. Since the drift length perpendicular to the beam is known (typically 2–5 mm) the recoil-ion transverse momentum or energy can be calculated. In order to reduce the influence of thermal motion, the target gas was cooled to 35 K. From systematic test experiments the accuracy of the energy determination in the spectrometer for small energies is estimated to be ±5 meV. A detailed description of the mechanical set-up, calculations on the solid angle and azimuthal angular acceptance as well as estimations on the influence of fringe fields in the spectrometer can be found in Ullrich *et al* (1991) and Dörner *et al* (1993).

4. Results

4.1. Total cross sections

The improvement obtained by incorporating a dynamical correlation in the CTMC method can be clearly seen from the results for total cross sections of helium single and double ionization in collisions with protons and antiprotons (table 1). The proton impact double ionization cross sections lie slightly below the earlier calculations by Montemayor and Schiwietz (1989), perhaps because of statistical error. The total cross sections for proton impact given by the dCTMC method for double ionization at 300 and 500 keV are 5 to 6.6 times closer to experiment than the four-body CTMC results employing independent electrons with initial binding energies of −0.896 au and the model potential given by equation (3) with λ_1 and λ_2 held constant at the value 1.6875. Even so, the absolute magitude of

double ionization by protons as obtained using the dCTMC method is still two to three times larger than the experimental data. The slight difference in single ionization cross sections between the two CTMC calculations as listed in table 1 is due to the difference in the double ionization cross sections. When the radial correlation is implemented, as expressed in equations (2) and (3), it decreases the probability of simultaneous ionization of two electrons by changing the screening factor which in turn increases the binding energy of one of the two electrons. On the other hand, when one electron is becoming more tightly bound than the initial state, the other electron sees no change in screening of the target nucleus and its ionization probability undergoes no change. Therefore, the decrease in the double ionization probability approximately adds up to the increase in the single ionization probability.

Table 1. Total cross sections (in units of 10^{-17} cm^2) for single (SI) and double (DI) ionization in 300 and 500 keV p, $\bar{p}$ + He collisions.

		CTMC	dCTMC	Expt
				Shah and Gilbody (1985)
300 keV	SI	3.72	4.04	5.40
p + He	DI	0.332	0.0731	0.0348
500 keV	SI	2.77	2.93	3.70
p + He	DI	0.245	0.0415	0.0172
				Andersen *et al* (1986)
300 keV	SI	3.07	3.27	
$\bar{p}$ + He	DI	0.308	0.0510	
500 keV	SI	2.36	2.51	2.55
$\bar{p}$ + He	DI	0.177	0.0265	0.025

We note that both single and double ionization total cross sections obtained by the dCTMC calculation for antiprotons colliding with He at 500 keV correctly predict the experimental results. However, since the dCTMC method overestimates the double ionization cross sections for proton impact, the larger ratio of double to single ionization by antiprotons as compared to the ratio using protons (Andersen *et al* 1986) does not emerge from the dCTMC calculation. The dCTMC calculation does provide a larger cross section for proton impact single ionization as compared to antiproton impact, the same result as given by Olson (1987). The latter calculation, in which the Bohr helium-atom model was employed and the explicit electron–electron interaction was included, predicts correct ratios of double to single ionization for both proton and antiproton impact, but the absolute double ionization cross section as a function of the impact energy decreases much faster than experiment as the energy increases. The difference in the two methods is that the dCTMC does not include the full correlation, i.e. the radial and angular correlation, between the electrons, whereas the Bohr helium-atom model does.

4.2. Differential cross sections for p + He collisions

4.2.1. Differential in projectile scattering angle. In figure 1, we compare the dCTMC results of single and double ionization cross sections differential in the projectile scattering angle with different sets of experimental data. Plotted for 500 keV impact are data of Giese and Horsdal (1988) for single and double ionization, Dörner *et al* (1989) for single ionization, and new results by Dörner and collaborators for double ionization. Data from Giese and

Horsdal (1988), Dörner *et al* (1989), Dörner (1991) for 300 keV impact are also plotted. At both energies, the dCTMC method produces an angular dependence on the projectile scattering angle θ_p that agrees with experiment over most of the experimental range for both single and double ionization. The total cross section for single ionization given by the dCTMC method is smaller than that of Shah and Gilbody (1985), and for double ionization the dCTMC result is about a factor of 2.4 too large. The differential cross section for single ionization given by the dCTMC method agrees with the data of Dörner and collaborators (1989), but lies above those of Giese and Horsdal (1988), and of Kristensen and Horsdal-Pedersen (1990) (not plotted). Such a discrepancy could be attributed to possible strong differences in the differential cross sections at small angles below $\theta_p \approx 0.25$ mrad. As mentioned by Kristensen and Horsdal-Pedersen, the data of Giese and Horsdal need to be adjusted upwards by 10% to 26%.

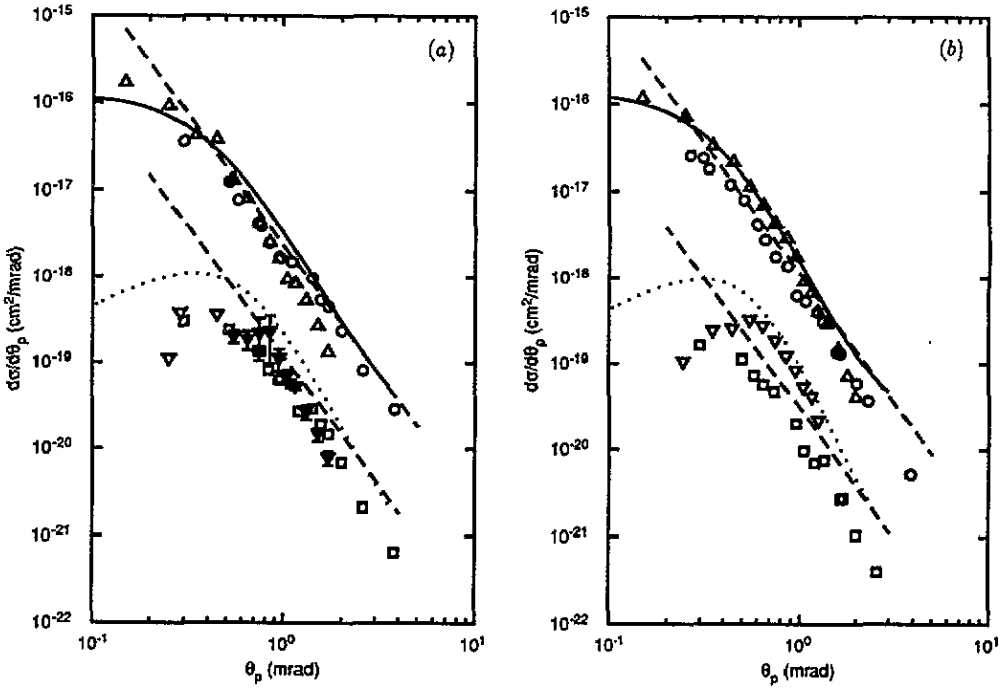

Figure 1. Cross sections for single and double ionization differential in the projectile scattering angle for collisions of protons with He at impact energies of (*a*) 300 keV and (*b*) 500 keV. Present calculation: full curve, single ionization; dotted curve, double ionization. Experimental results of Giese and Horsdal (1989): ○, SI; □, DI; Dörner *et al* (1989) at 500 keV and current work for 300 keV: △, SI; ▽, DI. The recent data of Kristensen and Horsdal-Pedersen (1990) are very close to those of Giese and Horsdal and are not plotted. The broken curves represent Coulombic θ^{-3} scaling and are normalized to the dCTMC results at large θ_p.

On the other hand, the theoretical double ionization cross section differential in the projectile scattering angle lies above the experimental data as expected since the integral cross section is overestimated. This is mainly due to the small angle behaviour of the double ionization cross section where the calculated results are above the experimental values at

both energies. The experimental cross section decreases for projectile scattering angles less than 0.5 mrad, whereas the dCTMC cross section reaches a maximum at about 0.3 mrad. Above 0.5 mrad, the present experimental results for double ionization agree with the dCTMC calculation at both energies and show a similar behaviour to that of Giese and Horsdal for 300 keV. The reason for the discrepancy between the experimental double ionization results at 500 keV is unclear.

Both single and double ionization tend to follow a straight line at large angles above 1 mrad (figure 1), which indicates that in this regime, the projectile scattering behaves like two-body central potential scattering (Rutherford scattering in the laboratory system) times an ionization probability $P(\theta_p)$ which is nearly constant,

$$\frac{d\sigma}{d\theta_p} = 2\pi \sin(\theta_p)\frac{d\sigma}{d\Omega_p} = 2\pi \sin(\theta_p)\frac{(Z_p Z_t)^2}{16E^2 \sin^4(\frac{1}{2}\theta_p)} P(\theta_p(b)). \tag{7}$$

In equation (7), b is the impact parameter and E is the impact energy of the projectile. Since the projectile scattering angle θ_p is of the order of 1 mrad, $d\sigma/d\theta_p \propto \theta_p^{-3}$. Deviations from the θ_p^{-3} scaling for the differential cross section are clearly seen for $\theta_p < 1$ mrad for both single and double ionization. This is partly due to an increasing dominance of the proton–electron momentum exchange at very small angles, $\theta_p \leqslant 0.3$ mrad, and to a decreasing ionization probability combined with increased screening of the target nuclear charge in the region of $\theta_p < 1$ mrad.

4.2.2. Charge-state fraction. Notice that in figure 1 the deviations from the θ^{-3} scaling are centred at different projectile scattering angles for the single and double ionization cross sections. These deviations, though hard to see, lead to a structure discovered by Giese and Horsdal (1988), when the charge-state fraction is plotted against projectile scattering angle, figure 2. Their experimental data and the data of Dörner and collaborators are shown in figure 2, together with the dCTMC results whose magnitude is divided by two. This factor is approximately the same factor that the dCTMC total double ionization cross section is larger than the experimental cross section (see table 1). The dCTMC results agree very well in shape with the experimental data, and are closer to the experimental results in their absolute magnitude than previous calculations with the independent electron approximation (Olson *et al* 1989, Salin 1991).

4.2.3. Transverse momentum transfer. We have further investigated the transverse momentum transfer associated with ionization for 300 and 500 keV impact energies, figure 3. The difference between the actual recoil-ion energy distributions and that of two-body scattering can best be illustrated by plotting the ratio of the average transverse recoil-ion energy, $\langle E_{R,\perp} \rangle$, to that of a two-body collision as a function of projectile scattering angle. The horizontal broken lines in figure 3 represent a two-body scattering by a central-force potential calculated from

$$\Delta k = k_p \theta_p \tag{8}$$

where k_p is the impact momentum of the projectile and Δk the transverse momentum transfer to the projectile. In the figures, the dCTMC results are compared with the experimental data of Dörner *et al* (1989) and present experimental data for both single and double ionization, and the eikonal distorted-wave calculation of Fukuda *et al* (1991) for 500 keV single ionization. The uncertainty in the experimental data is indicated by the scatter of the data

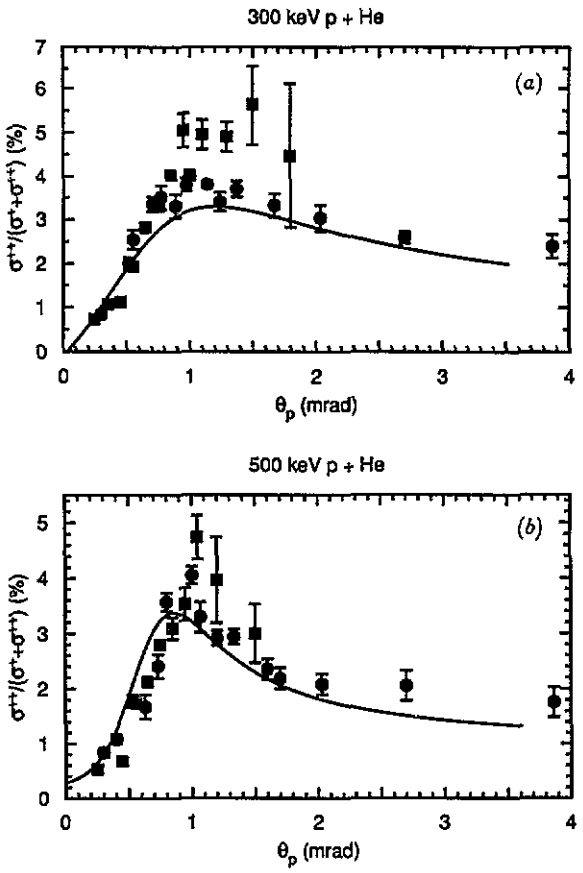

Figure 2. Charge-state fraction as a function of projectile scattering angle for collisions of protons with He at (*a*) 300 and (*b*) 500 keV. The full curve represents present calculation divided by two. Experiment of Giese and Horsdal (1989), ●, with error bars. Present experimental results: ■, with error bars.

for different independent measurements with various target geometries and materials which are denoted by the different symbols in the figure. The thermal motion of the target gas which was cooled to 30 K adds an average of $k_B T = 2.6$ meV to the mean energy of the recoil ion, $\langle E_{R,\perp} \rangle$. The data of Fukuda *et al* are plotted with the thermal motion of He already taken into account. The saturation energy of $\langle E_{R,\perp} \rangle$ obtained from small projectile scattering angles yields a value of about 3–4 meV for single ionization as given by the dCTMC calculation, which includes the thermal energy. This agrees with the CTMC result of Dörner *et al* (1991). Details of the experiment can be found in Dörner (1991), Dörner *et al* (1993) and Ullrich *et al* (1991).

Deviations from a two-body momentum transfer behaviour can be seen over the entire range of the projectile scattering angle. At large angles where the single differential cross sections were found to follow a θ_p^{-3} dependence, the scattering is indeed dominated by the interaction between the projectile and the He nucleus despite the fact that either one or two electrons are emitted. Between 0.3 and 1.5 mrad, recoil-ion energies are lower compared to those for two-body scattering. This indicates that in this region, the energy is preferentially transferred to ionized electrons instead of to the target nucleus. Such a behaviour is found to be more pronounced at the larger projectile energy. Theoretically as well as experimentally,

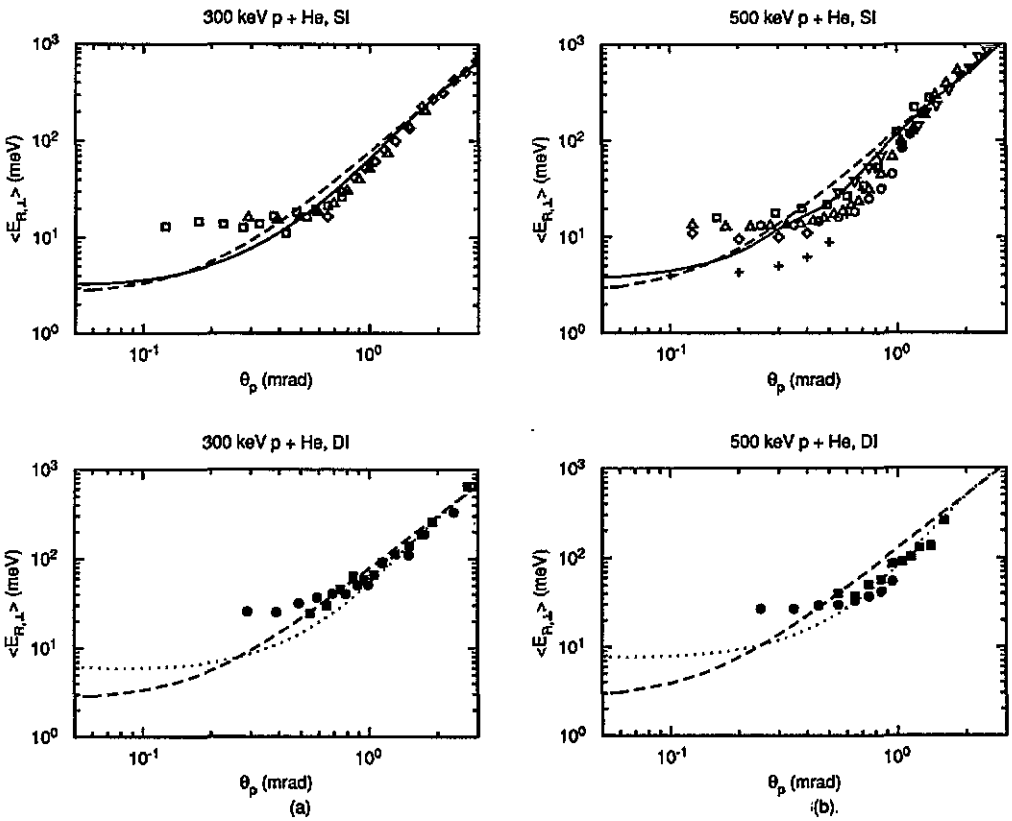

Figure 3. Ratio of the transverse recoil-ion energy in p + He collisions at (*a*) 300 and (*b*) 500 keV to that in two-body central potential collisions at the same impact energies. Present calculations: full curve, single ionization; dotted curve, double ionization. Experimental data of Dörner *et al* (1989): ▽, △, ◇, □, ○, single ionization; ●, ■, double ionization (different symbols denote results of independent experiments; scatter in the experimental data is due to unavoidable systematic errors in the determination of meV recoil-ion energies). The broken curves represent the two-body central-force scattering. Eikonal distorted-wave calculation by Fukuda *et al* (1991) for single ionization at 500 keV: +.

the ratios for single and double ionization show their maximum deviations from the two-body results at different projectile scattering angles, which is reasonable since additional momentum is transferred either to one or two electrons making a difference in the momentum balance of the heavy particles.

For projectile scattering angles below 0.2–0.3 mrad at both energies, experiment and the dCTMC calculations indicate that the recoil ions receive more momentum transfer from the ionized electrons than from the projectile. This can be seen as an indication that the interaction between the projectile and the target acts as a small perturbation compared with the interaction between the ionized electron and the recoiling nucleus. Both theory and experiment obtain larger recoil-ion energies at small projectile angles for double ionization versus that for single ionization. This can attributed to the fact that for double ionization an additional electron interacts with the target nucleus and that the momentum transfer to the recoil ion from two electrons in double ionization events does not average to zero. There is

still a considerable discrepancy between the theoretical and experimental values for $\langle E_{R,\perp} \rangle$ at small θ_p where the recoil-ion energy becomes independent of θ_p. From many independent experiments at different projectile energies, the measured low angle saturation value is found to be above theory by about 7 meV. The reason for this is unclear but may still be due to experimental problems since the discrepancy is very close to the absolute accuracy of the experiment, which is estimated to be ±5 meV. Presently, systematic measurements for electron impact are being conducted to explore this behaviour.

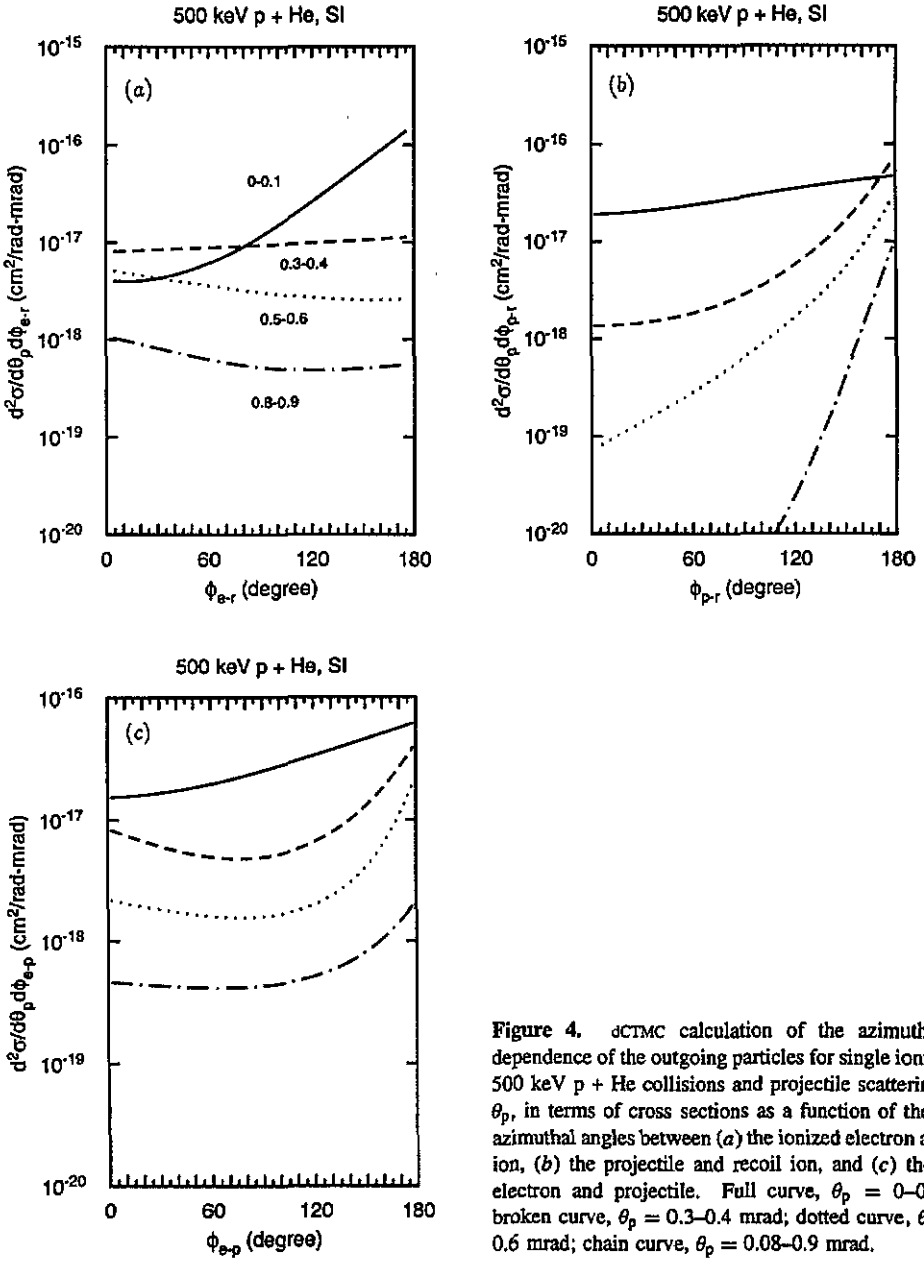

Figure 4. DCTMC calculation of the azimuthal angle dependence of the outgoing particles for single ionization in 500 keV p + He collisions and projectile scattering angles θ_p, in terms of cross sections as a function of the relative azimuthal angles between (*a*) the ionized electron and recoil ion, (*b*) the projectile and recoil ion, and (*c*) the ionized electron and projectile. Full curve, θ_p = 0–0.1 mrad; broken curve, θ_p = 0.3–0.4 mrad; dotted curve, θ_p = 0.5–0.6 mrad; chain curve, θ_p = 0.08–0.9 mrad.

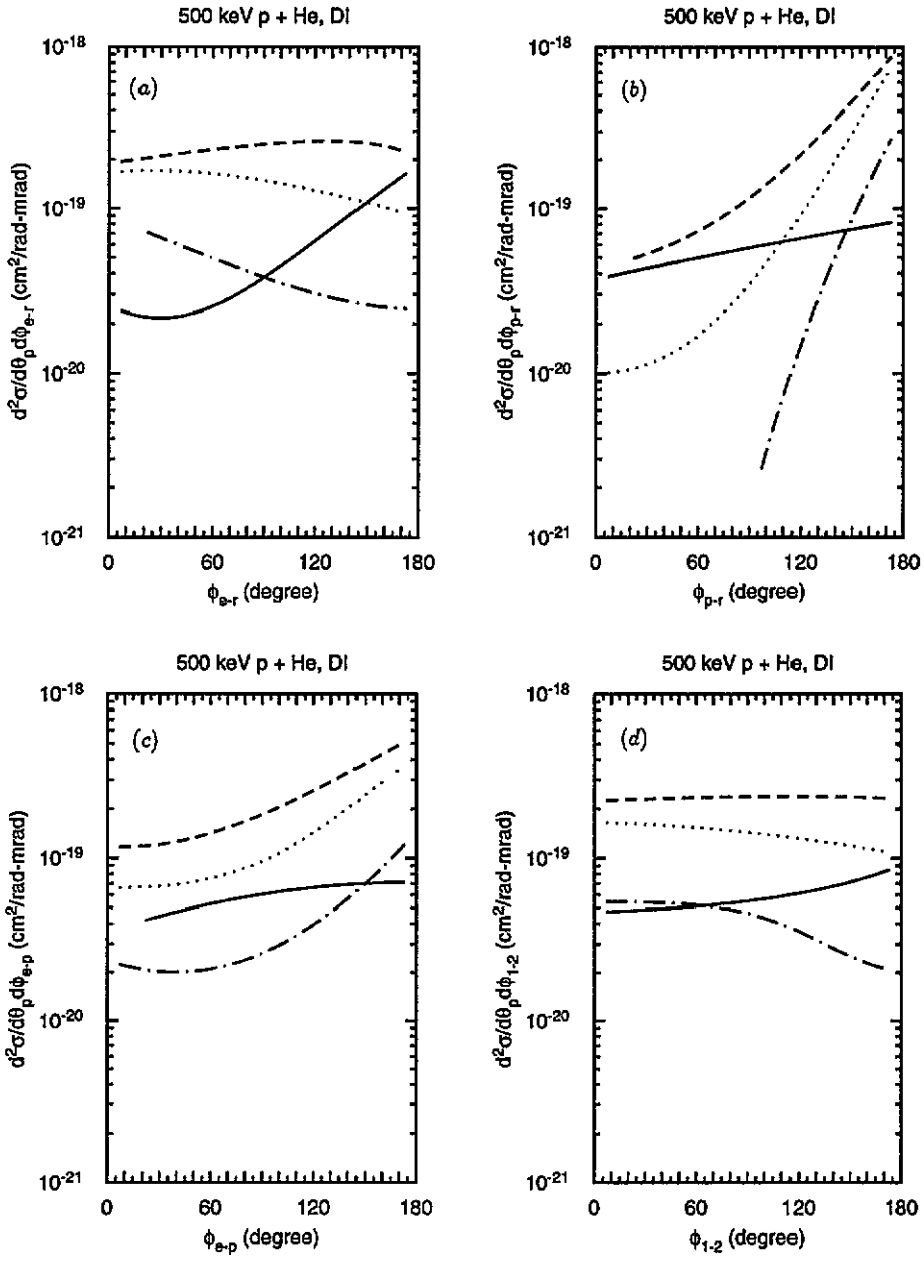

Figure 5. Azimuthal angle dependence of the outgoing particles for double ionization in 500 keV p + He collisions and projectile scattering angles θ_p, in terms of cross sections as a function of the relative azimuthal angles between (*a*) the ionized electron and recoil ion, (*b*) the projectile and recoil ion, (*c*) the ionized electron and projectile, and (*d*) the ionized electrons.

4.2.4. Azimuthal angular dependence. In order to understand the collision dynamics more fully, we show in figure 4 the azimuthal angle dependence of the outgoing particles for single ionization and projectile scattering angles of 0.0–0.1, 0.3–0.4, 0.5–0.6, and 0.8–0.9 mrad, in terms of the doubly differential cross sections as a function of the relative

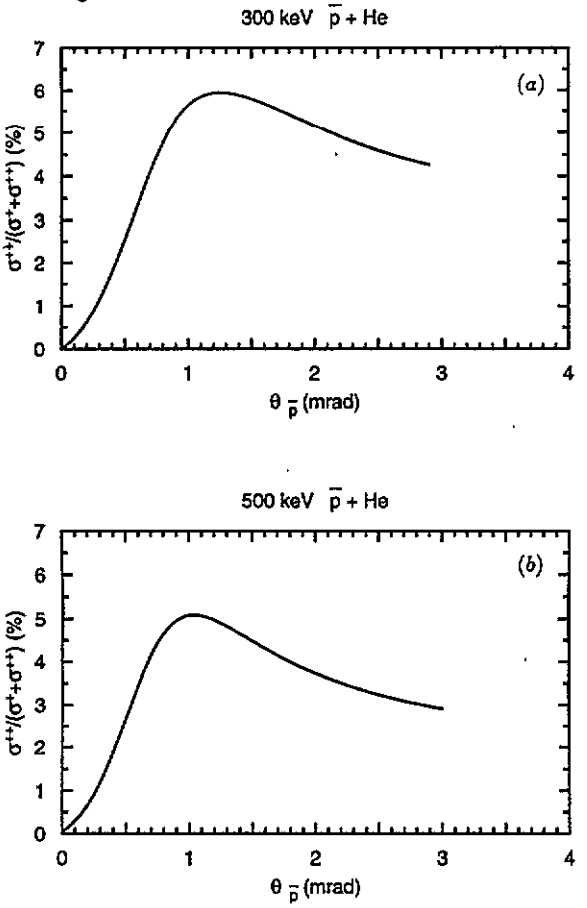

Figure 6. Present dCTMC calculation of charge-state fraction plotted against projectile scattering angle for (*a*) 300 keV and (*b*) 500 keV $\bar{p}$ + He collisions.

azimuthal angles between (*a*) the ionized electron and recoil ion, (*b*) the projectile and recoil ion, and (*c*) the ionized electron and projectile. Figure 4(*a*) shows that the ionized electrons are mainly scattered to the opposite azimuthal direction from the recoil ion for the smallest projectile scattering angles investigated but become more evenly distributed for larger projectile scattering angles. Figure 4(*b*), the scattering of the projectile relative to the recoil ion, shows an opposite situation to that in figure 4(*a*). This is consistent with the fact that larger projectile scattering angles correspond to closer collisions between the projectile and the target nucleus and therefore result in a central potential collision where the two nuclei are scattered with opposite momentum vectors. At the smallest projectile scattering angle, the projectile–recoil-ion azimuthal emission pattern is found to be evenly distributed which illustrates that in this regime momentum is mainly exchanged between the emitted electron and its parent nucleus. This is consistent with the observation of a saturation energy for small θ_p.

Figure 4(*c*), showing the scattering of electrons relative to the projectile, complements figures 4(*a*) and (*b*). It is interesting to note that the electrons also have a large probability of being scattered to the opposite azimuthal direction from the projectile. Thus, both the recoil ion and the electron momenta balance the transverse momentum of the projectile.

The azimuthal angle emission patterns for double ionization are displayed in figure 5. These patterns are similar to those for single ionization (figure 4) but they do show

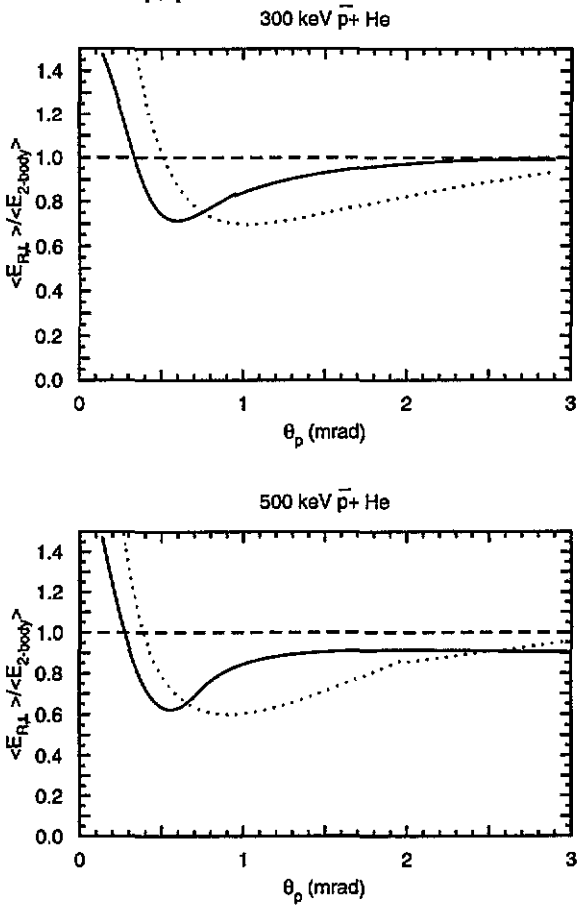

Figure 7. Ratio of the transverse recoil-ion energy in 300 and 500 keV $\bar{p}$ + He collisions to that in two-body central potential collisions at the same impact energies. Full curves, single ionization; dotted curves, double ionization.

some distinct differences. A broadening in the distribution of ionized electrons relative to the projectile is observed for large scattering angles. Since no shake-off contributions are included in our classical calculations, double ionization is solely due to consecutive interactions of the projectile with both electrons. Momentum is thus balanced between four outgoing particles which results in the observed broadening in the azimuthal distributions. It is also observed that ionization for projectile scattering angles of 0–0.1 mrad contributes relatively weakly to the total double ionization cross section compared to the contribution at larger projectile scattering angles, in agreement with figure 1.

Figure 5(*d*) shows the double ionization cross sections as a function of relative angles between the two outgoing electrons. Since no angular correlation is implemented in the dCTMC calculation, it is not unexpected that a nearly isotropic distribution results. This implies that the momentum transfer to the recoil ion from the emitted electrons does not average to zero. Both electrons may in fact be found on the same side opposite from the projectile. This is still compatible with the familiar picture that electrons repel each other since their velocities differ from each other. However, the calculations do not directly include the electron–electron interaction so these predictions probably overemphasize this effect.

4.3. Differential cross sections for $\bar{p}$ + He

The azimuthal angle dependence of the single and double ionization cross sections for collisions of antiprotons with He are very similar to those of protons, except for single ionization at small scattering angles. Very surprisingly, for $\theta_p \leqslant 0.1$ mrad, the electrons have a slight asymmetry to be scattered in the same direction as the projectile. A reason for this may be due to negative angle deflections of the antiproton from the Coulomb attraction with the recoil nucleus. The difference in ionization at small projectile scattering angle probably leads to the enhancement of single ionization for proton impact ionization as compared to antiproton impact ionization (see table 1) as well.

In figures 6 and 7, we show the charge-state fraction and the recoil-ion energy distribution as a function of the projectile scattering angle for 300 and 500 keV antiproton impact collisions with He. The behaviour is very similar to that obtained in the case of proton impact. No experiments have been performed as yet for the differential cross section and recoil-ion energy distribution in the collision of antiprotons with He. However, theory does indicate that a peak will be present in the angular dependence of the charge state fraction and strong differences from two-body scattering will appear in the recoil-ion momentum distribution.

5. Conclusions

In conclusion, the present study has utilized the dCTMC method, which includes radial electron correlation, to provide detailed information on several aspects of ionization of He, especially the momentum transfer involved in proton and antiproton collisions with He. With the inclusion of radial electron correlation in the two-electron system, the predictions made by the dCTMC method for single and double ionization total cross sections are close to experiment, especially for antiproton collisions. The recoil-ion energy distributions are very similar to those given by the conventional CTMC method. A difference between proton and antiproton collisions is found in the azimuthal angular dependence for single ionization at small projectile polar scattering angles.

Acknowledgments

Work supported by the Office of Fusion Energy, US Department of Energy, the National Science Foundation under grant no INT-9112815, and the Deutsche Forschungsgemeinschaft.

References

Abrines R and Percival I C 1966 *Proc. Phys. Soc.* **88** 861–72
Andersen L H, Hvelplund P, Knudsen H, Moller S P, Elsener K, Rensfelt K G and Uggerhoj J E 1986 *Phys. Rev. Lett.* **57** 2147–50
Cocke L and Olson R E 1991 *Phys. Rep.* **205** 153
Crothers D S F and McCarroll R 1987 *J. Phys. B: At. Mol. Phys.* **20** 2835–42
Deb N C and Crothers D S F 1990 *J. Phys. B: At. Mol. Opt. Phys.* **23** L799–803
—— 1991 *J. Phys. B: At. Mol. Opt. Phys.* **24** 2359–69
Dörner R 1991 *Thesis* University of Frankfurt
Dörner R, Ullrich J, Schmidt-Böcking H and Olson R E 1989 *Phys. Rev. Lett.* **63** 147–50

Dörner R, Ullrich J, Jagutzki O, Lencinas S, Schmidt-Böcking H and Olson R E 1991 Z. *Phys.* D S57–61
Dörner R, Ullrich J, Olson R J, Jagutzki O and Schmidt-Böcking H 1993 *Phys. Rev.* A **47** 3845–51
Fang X and Reading J F 1991 *Nucl. Instrum. Methods* B **53** 453–71
Fukuda H, Shimamura I, Végh L and Watanabe T 1991 *Phys. Rev.* A **44** 1565–76
Ford A L and Reading J F 1988 *J. Phys. B: At. Mol. Opt. Phys.* **21** L685–90
Giese J P and Horsdal E 1988 *Phys. Rev. Lett.* **60** 2018–21
Kristensen F G and Horsdal-Pedersen E 1990 *J. Phys. B: At. Mol. Opt. Phys.* **23** 4129–49
McGuire J H and Weaver L 1977 *Phys. Rev.* A **16** 41–7
Montemayor V J and Schiwietz G 1989 *Phys. Rev.* A **40** 6223–30
Olson R E 1987 *Phys. Rev.* A **36** 1519–21
Olson R E and Salop A 1977 *Phys. Rev.* A **16** 531–41
Olson R E, Ullrich J, Dörner R and H Schmidt-Böcking H 1989 *Phys. Rev.* A **40** 2843–6
Percival I C and Richards D 1975 *Adv. At. Mol. Phys.* **11** 1
Reading J F and Ford A L 1987 *Phys. Rev. Lett.* **58** 543–6
Reading J F, Ford A L and Fang Xushan 1989 *Phys. Rev. Lett.* **62** 245–8
Reinhold C O and Falcón C A 1986 *Phys. Rev.* A **33** 3859–66
Salin A 1989 *J. Phys. B: At. Mol. Opt. Phys.* **22** 3901–14
—— 1991 *J. Phys. B: At. Mol. Opt. Phys.* **24** 3211–8
Schultz D R, Olson R E and Reinhold C O 1991 *J. Phys. B: At. Mol. Opt. Phys.* **24** 521–58
Shah M B and Gilbody H B 1985 *J. Phys. B: At. Mol. Phys.* **18** 899–913
Ullrich J, Dörner R, Lencinas S, Jagutzki O and Schmidt-Böcking H 1991 *Nucl. Instrum. Methods* B **61** 415–22